Materials Research. 2023; 26(suppl. 1):e20220520
DOI: https://doi.org/10.1590/1980-5373-MR-2022-0520

Use of the Arduino Platform for the Piezoresistivity Analysis in Self-Sensing Cement Composites

João Batista Lamari Palma e Silva[a]*, Rosa Cristina Cecche Lintz[a], Luísa Andréia Gachet[a]

[a]Universidade Estadual de Campinas, Faculdade de Tecnologia, Programa de Pós-Graduação em Tecnologia, Limeira, SP, Brasil.

Received: December 05, 2022; Revised: July 26, 2023; Accepted: October 20, 2023

Concrete structures are susceptible to several factors during their life cycles, which can cause various problems. This situation can be avoided in many cases if Structural Health Monitoring (SHM) is used. However, such monitoring is often expensive due to the large number of sensors and the use of data acquisition systems (DAQ). In this context, self-sensing cement composites (SSCCs), monitoring themselves without sensors by incorporating conductive fillers in their composition, provide a better piezoresistive effect. In this research, the Arduino platform and analog to digital converters (ADC) modules were tested, and a prototype of a low-cost DAQ was developed for monitoring SSCCs. The devices were analyzed from the compression tests on the mortar specimens, and the results were compared to measurements obtained from the reference equipment (professional DAQ). The results showed a good sensitivity and an adequate correlation between both devices in some cases. It showed that the Arduino platform has the potential to be used in the experimental monitoring of SSCCs, however it needs to be combined with an ADC module.

Keywords: *Structural monitoring, self-sensing cement composites, piezoresistivity, Arduino platform.*

1. Introduction

The great advances in the technology of concrete production, such as ultra-high performance concrete, has been used in construction such as skyscrapers and marine construction, in addition to those such as large bridges, tunnels, and highways. Such constructions are exposed to a variety of factors during their life cycles, such as aging of materials, wind loading, ocean waves, and earthquakes, or even the variation in loading caused by inappropriate use of constructions. These situations often cause damage to the structure, which manifests itself in the form of corrosion, cracking, and disintegration, as well as strain and excessive displacement. These manifestations often can promote the occurrence of the collapse of the structure, and several of these collapses could be avoided if there was adequate monitoring of the structure[1-3].

Most of the time when Structural Health Monitoring (SHM) is used, several sensors have been used, which can be expensive. In addition, these sensors can cause, in some situations, the loss of mechanical properties of the structure when they are embedded in the structure. Therefore, sensors that do not harm the mechanical properties of the structure, as well as are low-cost, and have a long service life, can solve the disadvantages of current sensors[4,5].

To solve such disadvantages in SHM, researchers are increasingly interested in the use of self-sensing cement composites, which consist of a material able to feel itself without the need to install embedded or coupled sensors, promoting multifunctionality to the composite. Thereby, in addition to performing its elementary function as a building material, the composite monitors itself, without losing its mechanical properties and without reducing its durability[2,6].

Although the use of self-sensing cement composites is currently attracting more and more attention from researchers, it has been studied since the early 1990s, when researchers Chen and Chung published their findings, making 1993 a milestone for the beginning of the subject. It was the time when studies involving the self-sensitivity of concrete with carbon fibers began by measuring its piezoresistivity compared to strain caused by mechanical forces[2,7,8].

However, even though great progress has been achieved in the field of SHM, there is still a need to overcome several challenges so that self-sensing cement composites can be effectively used on a large scale in monitoring structures. Currently, researchers are concerned about the behavior of these materials on issues such as the relationship of their characteristics with electrical resistivity, which leads to the need for more studies and analysis before they can be used in large real structures[9,10].

Beyond the challenges involving advances in technology for the development of self-sensing concrete, other barriers also make it difficult to use, such as the hardware and software used in the Data Acquisition Systems (DAQ) of SHM. These systems have a high cost for purchase and they usually are not open-source code, that makes it impossible for them to be freely reproduced[11,12].

In general, the high cost and complexity of operations involving the use of DAQ (hardware and software) means

*e-mail: lamaripalma@hotmail.com

that there is a limit to their use by researchers. Therefore, the development of an open-source system can help the expansion of the use of SHM[11,13], including the monitoring of SSCCs.

Several researchers have used low-cost microcontrollers in experiments involving physical quantities, including some associated with SHM, such as strain measurement, acceleration, and electrical resistivity. Part of these researches (Table 1) uses the Arduino platform, due to its low-cost and relative ease of operation, as well as its possibility of integration with the Internet of Things (IoT)[15,21-24]. In addition to Arduino, other platforms such as the Raspberry Pi, ESP-8266, and Beagleboard are also frequently used by researchers in the field of SHM[25-28].

In the field of electrical resistivity analysis, Cardona-Vivas et al.[29] used the Arduino platform to evaluate the piezoresistivity of a sensor developed based on acrylic resin with the incorporation of waste from electric batteries. Another application of the Arduino platform involving electrical resistivity was developed by Birgin et al.[30], which used the platform in a weight detection system for vehicles in motion on a self-sensing asphalt pavement. Both researchers found promising results with the use of the Arduino platform for self-sensing analysis.

The scientific literature on the uses and applications of the Arduino platform is vast and almost inexhaustible. Certainly, its use may imply limitations and disadvantages. However, the Arduino platform already presents itself as an advantageous tool in the field of electronic prototyping[31]. The only uses of the Arduino in self-sensing cement composites (SSCCs) experiments are only related to using the platform to supply voltage or to transfer data[32-35]. Despite the countless applications registered in the literature about the use of Arduino in SHM, its use and the development of a low-cost system for monitoring SSCCs based on the piezoresistive effect were not found.

Therefore, this paper shows Arduino's tests and complementary modules, as well as the development of a prototype of a low-cost system for monitoring SSCCs based on the piezoresistivity effect. It was made with open-source hardware and software.

2. Self-Sensing Cement Composites Based on Piezoresistivity

Cementitious composites, such as concrete and mortar, are considered insulators in terms of their ability to transmit electrical energy. Therefore, conductive materials are incorporated into cementitious composites, which allow good electrical conductivity, as well as the occurrence of the piezoresistivity effect, which allows the increase of the ability to detect mechanical stresses and strains through the self-sensitivity of the composite. Therefore, self-sensing cementitious composites become multifunctional since the addition of conductive fibers, in addition to improve the piezoresistive effect, can also increase other properties of concrete and mortar, such as increased strength, greater ductility, and improved durability[2,36].

Several types of fibers, such as those made from polymers, glass, and carbon, have been used in the production of cement composites to improve the physical properties of fresh and hardened concrete. However, fibers based on polymers and glasses are considered insulating materials for electricity. In other words, they are not useful in the manufacture of concrete that seeks self-sensitivity through the change of electrical resistivity, which is the case of carbon fibers and steel, which have good electrical conductivity[37].

The fillers that compose the piezoresistive material can be either fibers or particles. In the case of fibers, they can be long or short, which characterizes their discontinuity. In addition to the presence of porosity and internal water in the concrete, the placement of fillers is another important factor in the piezoresistivity mechanism[37], as illustrated in Figure 1 elaborated from[38,39].

It is not only the conductive filler that will influence the piezoresistivity of self-sensing concrete but also other variables, especially those related to concrete rheology, such as water/cement ratio, chemical additives, and characteristics of conventional aggregates, since they directly interfere in the dispersion of the conductive filler with the composite and consequently change the electrically conductive paths[40].

Also based on Figure 1, when the specimen has a strain from uniaxial compression, the fibers and particles come closer, creating longer electrically conducting paths than those existing before the strain. This situation causes the electrical current to increase due to the higher conductivity, from the reduction of the electrical resistance, which characterizes the effect of piezoresistivity on SSCC[2].

To analyze the resistivity, it is recommended that the metallic electrodes be embedded (Figure 2, elaborated from[41,42]) in the cementitious composite, which also helps to reduce the noise since they are unavoidable in measurement processes of electrical quantities[43].

For piezoresistivity analysis, it is necessary to determine the electrical resistivity (ρ) as the change of compression load

Table 1. Applications with Arduino in SHM.

Arduino model	Application	Quantity properties	Reference
Genuino	Concrete slab	Acceleration (vibration)	Nunes et al.[14]
Mega	Concrete beams	Strain, force and displacement	Silva et al.[15]
Nano	Metallic stair	Humidity, temperature, acceleration (vibration), strain and impact	Malik et al.[16]
Uno	Small-scale bridge model	Acceleration (vibration)	Patel et al.[17]
Uno	Railway bridge	Acceleration (vibration)	Ozdagli et al.[11]
Uno	Concrete beams	Acceleration (vibration)	Khan et al.[18]
untold	Joint in steel frame	Acceleration (vibration)	Serdjuks et al.[19]
ProMini	Concrete blocks	Sonic speed of propagation	Misra et al.[20]
Due	Aluminium cantilever	Acceleration (vibration)	Buckley et al.[21]

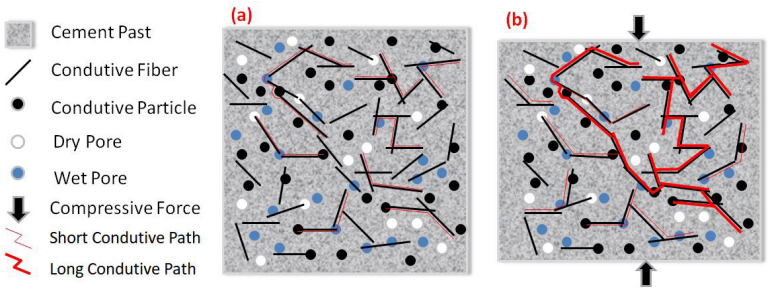

Figure 1. Scheme of self-sensing cement without load (a); with load compression (b).

applied to the structure or specimen occurs. From Ohm's Law, it is possible to obtain the electrical resistance (R) and consequently the resistivity (ρ) according to Equation 1 adapted from[44,45]. The values of the contact area (A) of the electrodes with the composite and the distance (L) between them are all known (Figure 2).

$$\rho = \frac{RA}{L} \tag{1}$$

However, the SSCCs based on the effect of piezoresistivity are not restricted only to the property of offering electrical resistance. They also have characteristics related to electrical capacitance[46], a situation that makes SSCCs not purely ohmic materials. Due to their capacitance property, SSCCs suffer from the polarization effect, causing a delay in the stabilization of the electrical resistance, similar to the behavior of capacitors[41]. The polarization effect is due to the movement of free ions in the pores of the cement matrix when subjected to an electric field. Negative and positive ions move towards the electrodes, separating from the center of electrical charges. This movement generates an electric field in the opposite direction to the current flow, which causes the electrical resistance to increase over time[47].

Thus, only when complete polarization of the composite occurs, its resistance can be estimated from Ohm's Law[48]. Otherwise, the measurement results may be impaired due to the polarization effect. This effect can be avoided by using alternating current (AC) or biphasic DC[6,49].

One of the types of electrical circuits that can be used to measure electrical resistance in SSCCs is that in Figure 3 elaborated from[36], where the electrical resistance of the composite (R_C) is determined using Equation 2 adapted from[41,50]. The values of a fixed reference resistor (R_{ref}), electrical supply voltage (U_{in}) of the circuit, and the electrical voltage between electrodes embedded in the composite (U_c) are all known.

$$R_C = R_{ref}\frac{U_c}{U_{in} - U_c} \tag{2}$$

After determining the R_C, it replaces R in Equation 1 and the electrical resistivity (ρ) of the composite is obtained. Therefore, the sensitivity of the piezoresistivity can be analyzed through strain (ε) by the Equation 3 adapted from[51,52], where K is the gauge factor. As an alternative, the

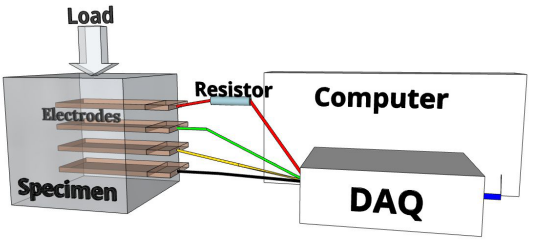

Figure 2. Electrical resistance measurement scheme in a piezoresistive specimen with embedded electrodes.

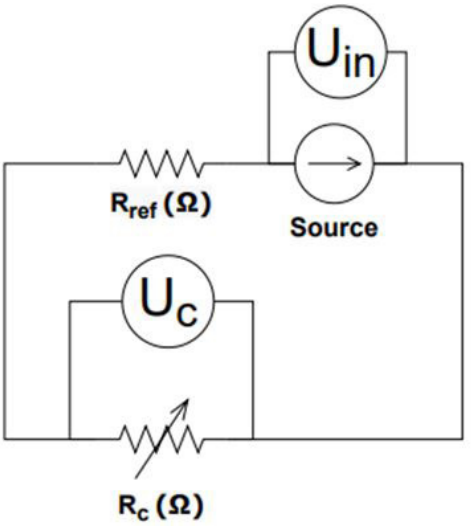

Figure 3. Circuit for measuring electrical resistance in piezoresistive composites.

sensitivity can also be analyzed through stress (σ) through Equation 4 adapted from[53-55], where SS is the stress sensitivity.

$$K = \frac{\frac{\Delta\rho}{\rho_0}}{\varepsilon} \tag{3}$$

$$SS = \frac{\frac{\Delta\rho}{\rho_0}}{\sigma} \tag{4}$$

The piezoresistivity analysis is commonly showed in the literature through Equation 5 adapted from[45], where the Fractional Change in Resistivity (FCR) value is obtained.

$$FCR\% \quad \frac{\rho}{\rho_0}100 \tag{5}$$

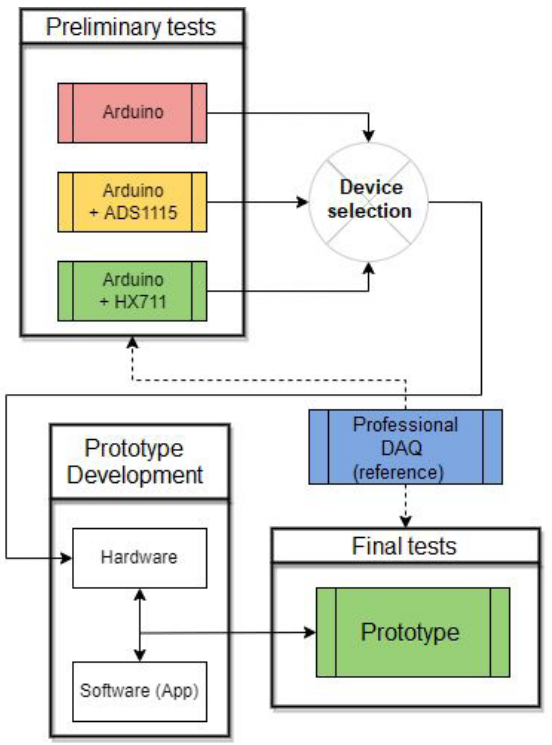

Figure 4. Flow of experimental stages.

The FCR value is used for comparing the mechanical stress, strain, and force applied to the structure or specimen, to verify the piezoresistive effect, as well as to obtain, in some cases the gauge factor of the composite.

3. Materials and Methods

This work consisted of three experimental stages (Figure 4). The first stage was the execution of preliminary tests that led to the selection of the most suitable hardware components for the development of the prototype, which was the second stage. Lastly, the third stage included the prototype tests. However, even before these stages, mortar specimens were prepared with the characteristics described below (section 3.1.).

A professional DAQ (Micro-Measurements, model: 8000-8-SM) was used as a reference to compare the results of the preliminary tests and the prototype tests.

3.1. Specimens preparation

Mortar mix proportions were produced, with the composition indicated in Table 2. Graphite was used to make the mortar more electrically conductive, so that the piezoresistive effect could be better seen.

According to the manufacturers, the specifications of the raw materials (Figure 5) used were: Portland Cement (marketed by Votorantim Cimentos) Classification CP-II-F-32; Graphite powder (marketed by Wonder Company), carbon (loss to fire) >72%; ash at most 28%; maximum humidity 0.5%; Sand type was from quartz.

The physical properties of the raw materials are indicated in Table 3, and the granulometric analysis of the sand and graphite is shown in Figure 6.

The preparation of the mortar consisted of manually mixing the raw materials. The molding and curing of the

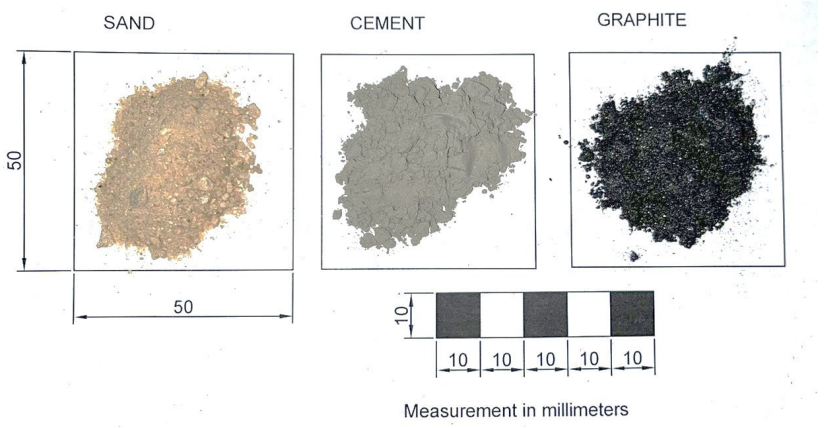

Figure 5. Sample of raw materials utilized in mortar production (measurement in millimeters).

Table 2. Mix proportions of the mortar in terms of cement mass.

ID	Cement	Sand	w/c ratio	Graphite
T0	1	4	0.50	0
TG	1	4	1.05	0.25

mortar's specimens (Figure 7) followed the Brazilian standard NBR 16868-2[59], for cubic specimens, with dimensions of 40 x 40 x 40 mm^3, used in compression tests.

Table 3. Physical properties of the raw materials.

Properties	Cement	Sand	Graphite
Specific mass [g/cm^3]	2.95[a]	2.64[b]	2.41[a]
Unit weight [g/cm^3]	0.91[d]	1.48[c]	0.38[d]
Maximum diameter [mm]	-	4.80[e]	0.15[e]
Fineness modulus	-	2.03[e]	0.25[e]

Reference standards: [a]NBR 16605[56]; [b]NBR 16916[57]; [c]Chapman vessel; [d]No standardization; [e]NBR 17054[58]

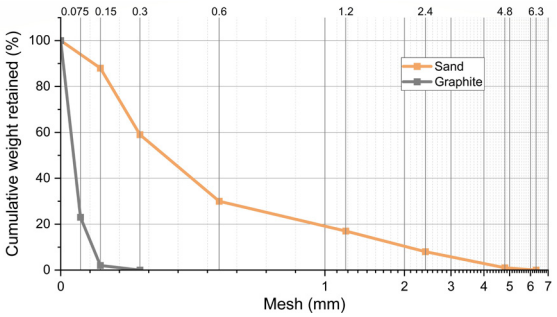

Figure 6. Granulometric distribution (standard NBR 17054[58]) of sand and graphite particle sizes.

During the molding of these specimens, 4 aluminum electrodes with dimensions of 35 x 20 x 0.1 mm^3 each were used, of which 35 mm in length, 25 mm embedded in the mortar, giving a contact area of 50 mm^2 with the mortar. The electrodes were spaced 10 mm between them. In each of the specimens, a strain gauge of 120 Ω was installed (Figure 8), so that it was possible to compare the effect of piezoresistivity with the strain.

After the curing process (28 days), no drying process was performed on the specimens before the tests.

3.2. Setup of compression tests

As these are non-destructive tests, a manual press system was used, where the specimens were arranged as shown in Figure 9.

Reference values of force (F) from the load cell and strain (ε) from the strain gauge were collected simultaneously by a reference DAQ for further analysis in comparison to the data obtained by the devices (Arduino, ADS1115 and HX711) or the prototype presented in this work. The sampling rate used for all data acquisitions was 10 Hz. The maximum force applied was approximately 2 kN, as that is sufficient intensity to cause the piezoresistive effect in the samples[60], as well as not to cause their rupture, as they are non-destructive tests.

The relationship between quantities (bytes, voltage, force, and strain) was verified by using the Pearson Correlation (r) analysis[61], coefficient of determination (R-Square) and sensitivity (S) of the piezoresistivity according to Equations 6 and 7 adapted from Equations 4 and 5. A statistical analysis was performed with analysis of variance (ANOVA one-way)

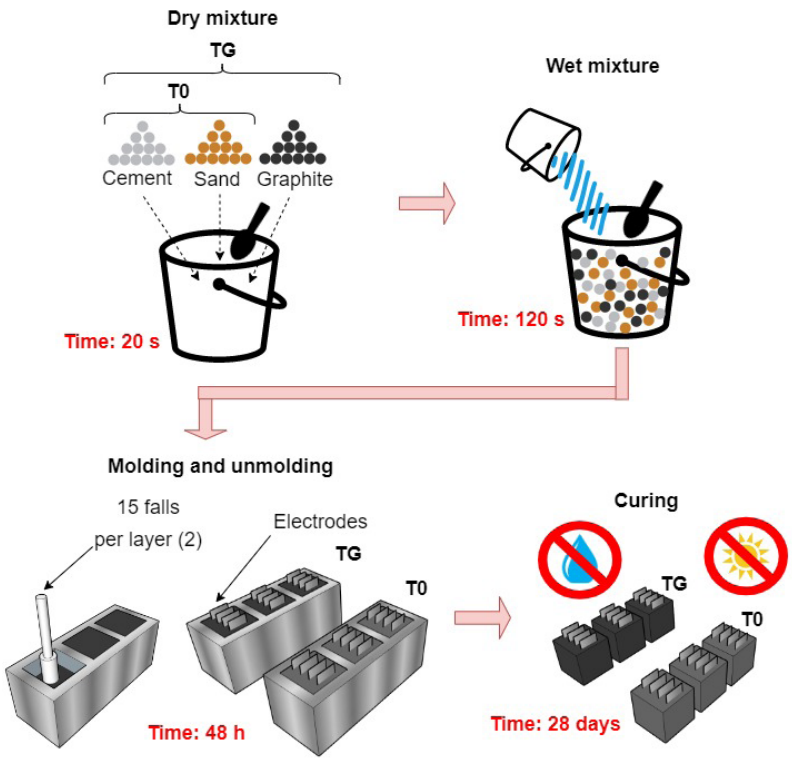

Figure 7. Mortar and specimen preparations.

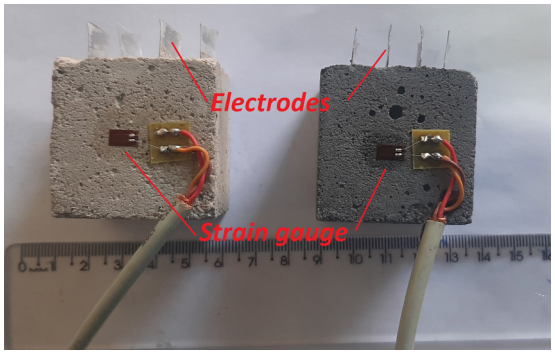

Figure 8. Specimens with electrodes and strain gauges installed.

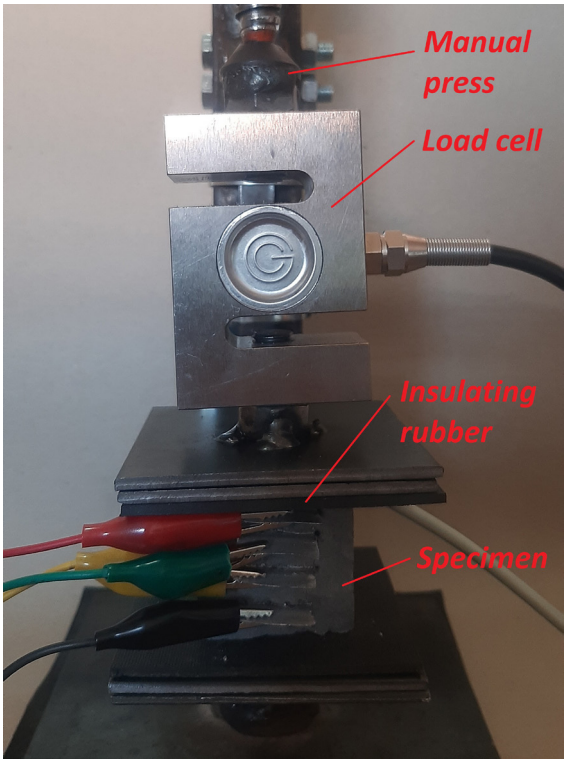

Figure 9. Setup of compression tests.

followed by the Tukey Test, where a $p<0.05$ was considered to indicate a statistically significant difference. These analyses were performed using OriginLab Pro software, version 2022b.

$$S_{bytes} = \frac{\Delta \text{ Bytes}}{\Delta\sigma} \quad (6)$$

$$S_{stress} = \frac{FCR}{\Delta\sigma} \quad (7)$$

3.3. Devices preliminary tests (Arduino, ADS1115 and HX711)

The Arduino electronic prototyping platform was selected due to its low-cost, relative ease of use, and because it is an open-source platform, as well as the ADS1115 and the HX711 modules, which are low-cost analog-digital converters (ADC).

Initially, only the Arduino electronic prototyping platform model UNO R3 was tested, without the use of any of the additional modules. Two analog ports (A0 and A1) were used to measure the differential change of electrical voltage between 0-5 V, which performs an analog-digital (AD) conversion in 10 bits. Then, together with the same Arduino, the ADS1115 analog-digital converter module was used, which performs conversion in 16 bits. Finally, the analog-digital converter module HX711 was used together with the same Arduino, which performs conversion into 24 bits. In these three devices, the voltage source of the measurement circuit (Figure 3) was provided by direct current (DC).

The tests with each of the three devices were conducted through compression tests on cubic specimens, with comparison between the values in bytes resulting from the change in electrical voltage measured at the electrodes caused by the piezoresistivity effect. This value in bytes was compared to the force (F) and strain (ε) readings collected simultaneously by the reference DAQ for further analysis.

Based on the preliminary results, the HX711 module was chosen for the prototype shown in this article.

3.4. Prototype development

In the initial tests described in section 3.3, with results presented in section 4.1, the values of the digital data were limited to the use of bytes, thus, there was no conversion to electrical quantities like those used in the piezoresistivity analysis. For the conversion to be possible in these units, it was necessary to use reference resistors (R_{ref}), with an arrangement according to the circuit shown in Figure 3.

However, since it is a reference resistance value that may need changes for certain reading values, five metalfilm resistors were inserted in the circuit, in the following values 1 kΩ, 10 kΩ, 100 kΩ, 1 MΩ and 10 MΩ (component #2 of Figure 10), which are switched using a selector switch (component #1 of Figure 10 and Figure 11a). To reduce the noise inherent to measurement systems, a 1 µF multilayer ceramic capacitor (component #3 in Figure 10) was installed at the closest electrical power supply to the specimen.

The initial circuit, consisting of components #1 to #5 in Figure 10, connects to the HX711 module and this to the Arduino, which transfers the information via serial communication (RX/TX) to the HC-05 Bluetooth module (respectively components #7, #8 and #6 of Figure 10). In the final version of the prototype, the Arduino NANO module was used, so that it was possible to reduce the size of the system.

An independent DC power supply system was used for the Arduino/HX711/LED and another for the HC-05 Bluetooth module, to avoid any type of voltage/current change that could oscillate the measurements, once only one power supply (Hi-Link-PM01) module (component #11 in Figure 10) there was an oscillation in the circuit supply. However, there are other ways (filtering, bypassing, or post-regulation the signal) to solve this problem, aiming to use only one power supply, which was not the goal of this research.

For the operation of the prototype, a mobile app was developed to be used on smartphones or tablets. This software (app) was

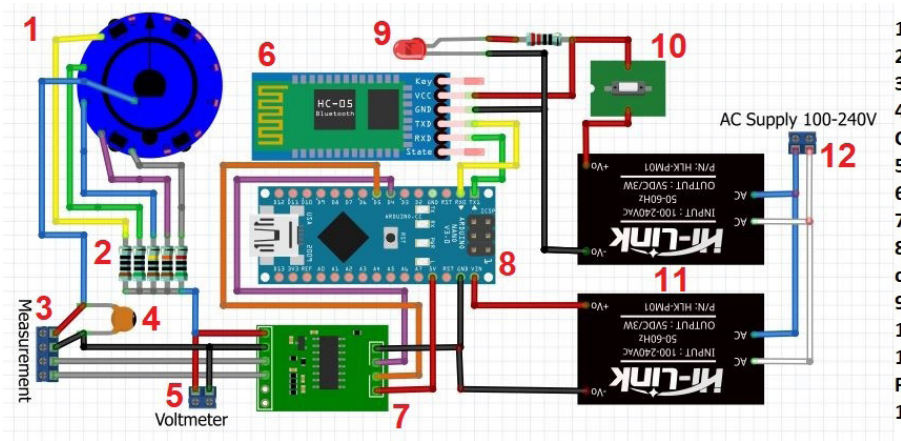

Figure 10. Prototype hardware design with Fritzing software.

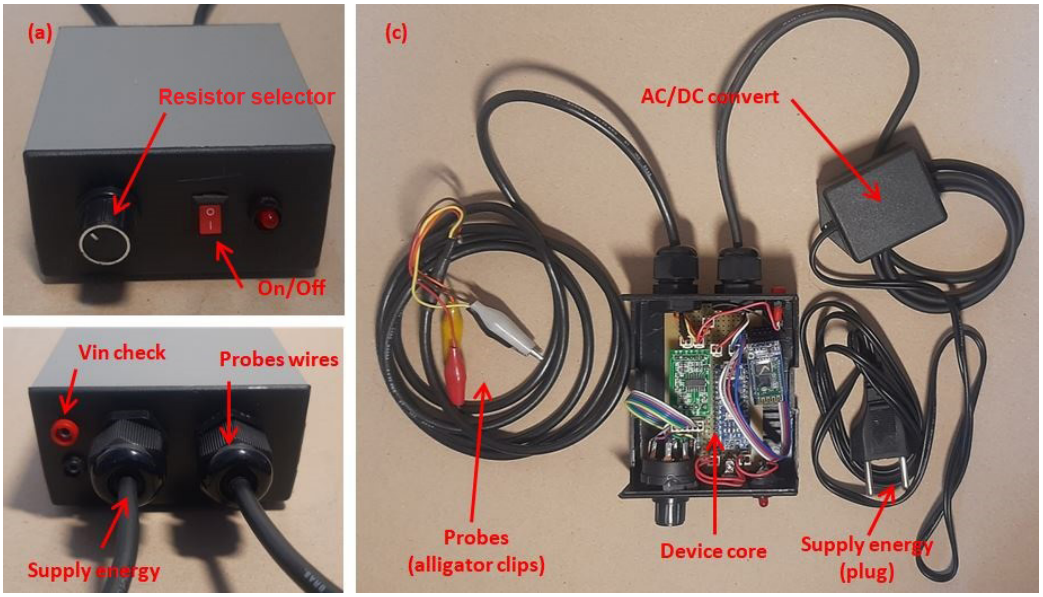

Figure 11. Hardware of the prototype developed.

developed using the App Inventor online platform, which is maintained by the Massachusetts Institute of Technology (MIT).

Figure 12a shows the flow of data, which arrives in the form of a digital signal in bytes, transferred from the prototype's hardware to the smartphone (or tablet) through a wireless transmission of the Bluetooth (BT) type. The value in bytes is converted into voltage and resistance until the resistivity is found, which is based on other factors, such as the values that are inputted on the user interface screen (Figure 12b).

Also, in the app's data acquisition screen (Figure 12b), the recording (in the smartphone's internal memory) of the results displayed on the screen can be activated by activating the "Record" switch. Once these data have been recorded, they can be exported in the Comma Separated Values (CSV) format for use in spreadsheet software such as MS-Excel.

As it is an open-source system proposal, the firmware programming codes for use in Arduino NANO or UNO, as well as the app software (for smartphones and tablets with Android OS), are available in supplementary data.

3.5. Tests with the developed prototype

Before the tests of the prototype, due to the scarcity of information in the literature about prototypes applied to piezoresistivity analysis in self-sensing cementitious composites, reference parameters were established. These parameters were determined from tests conducted only with the reference DAQ, which were compared to each other in the following cases: FCR (piezoresistivity) *versus* applied force (F); and FCR *versus* strain (ε).

After establishing such reference parameters, the same specimens were tested using the prototype developed, through the acquisition of electrical voltage by the prototype and other quantities (force and strain) by the reference DAQ.

4. Results

The results below were divided into two sections. The first section (4.1) shows the preliminary testing stage that led to the choice of the converter module used in the prototype development. The second section (4.2) presents the results of the prototype tests.

4.1. Preliminary test results

The test with mix proportion T0 for measuring electrical change due to piezoresistivity caused by compression was almost imperceptible in the case of the use of an Arduino for the strain response and applied force, as shown in the graph in Figure 13a. In the case of the same test, but with the mix proportion TG, there was a graphically perceptible piezoresistive response, as shown in Figure 13b, which is suggested to have occurred due to the addition of graphite.

Afterward, the tests were redone using the ADS1115 module together with an Arduino. In the case of the mix proportion T0, there was a significant increase in the graphic perception (Figure 14a) of the piezoresistive response compared to the results obtained only with the use of Arduino (Figure 13). This was probably due to the higher resolution in the AD conversion rate of the module, in this case 16 bits. In the same test, but with the TG mix proportion, the piezoresistive response was close to the compression force used, as shown

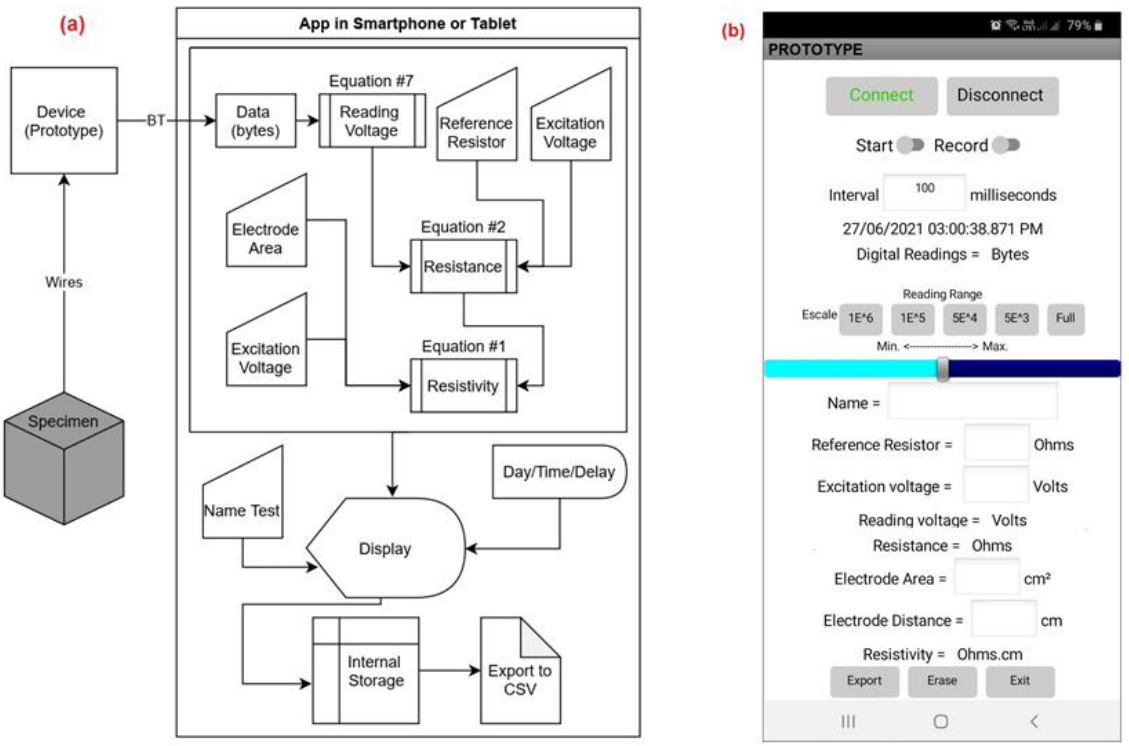

Figure 12. Information flow in the app (a) and the app's data acquisition screen (b).

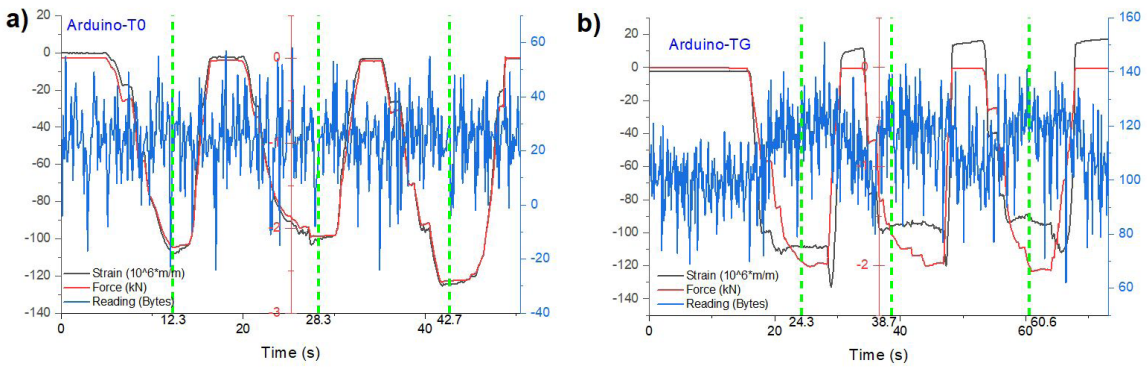

Figure 13. Arduino without complementary module in compression test with mix proportions T0 (a) and TG (b).

in Figure 14b. This happened because graphite was added to the mix.

The graphic results of the tests using the HX711 module with Arduino are presented in Figure 15. In the case of the mix proportion T0, there was a significant increase in the graphic perception (Figure 15a) of the piezoresistive response compared to the results obtained only with the use of Arduino (Figure 13) and the ADS1115 module (Figure 14). This was probably due to the higher resolution in the AD conversion rate of the module, in this case, 24 bits. Therefore higher resolution provided by the use of the HX711 module, the graphic results between T0 and TG (Figure 15b) were visibly close between them, but the sensibility of the TG was higher than the T0, due to the addition of graphite.

The results of the sensitivity analysis between the electrical and mechanical variations of each device (green lines in Figures 13, 14 and 15), show (Table 4) an increase in sensitivity with the increase in the AD conversion rate, as well as between the mix proportions T0 and TG.

The piezoresistive effect that occurred in the control mixture (T0) has also been observed in other studies[62-65]. Some researchers[42,66] evaluated the moisture in the specimen, which can explain the piezoresistive response of the mix proportion T0 (without graphite).

The analysis of variance (ANOVA one-way) was performed separately for each device, using the sensitivity values from Table 4. The results are shown in Table 5, indicating that some means are different (p-value<0.05) at a level of 95% significance.

The Tukey's Test of the sensitivity values showed a significant difference in mean, especially in the case of the HX711 when compared to the other devices and between the T0 and TG mix proportions, as shown in Figure 16.

In addition to the graphical and statistical analyses, the Pearson's correlation and R-squared results in Figures 17 and 18, also show a better result for the HX711 module. In all cases of these results (Arduino, ADS1115, and HX711), the mix proportion with graphite (TG) gave a better response than without graphite (T0).

In all tests with the HX711 module, it was found that there was an increase in noise in the readings when touching the manual press, to make the compression, which was reduced by using insulating gloves.

In the case of using the ADS1115 module, although the correlation results by Pearson analysis were not satisfactory when compared to the use of the HX711, the graphic response (Figure 14) showed a better visual correlation between piezoresistive effect and mechanical compression effect (force and strain), which was not found in the case of using Arduino without any additional modules.

4.2. Test results of the prototype developed

With the system prototype (hardware and software) made, it was initially tested to verify the polarization effect in comparison

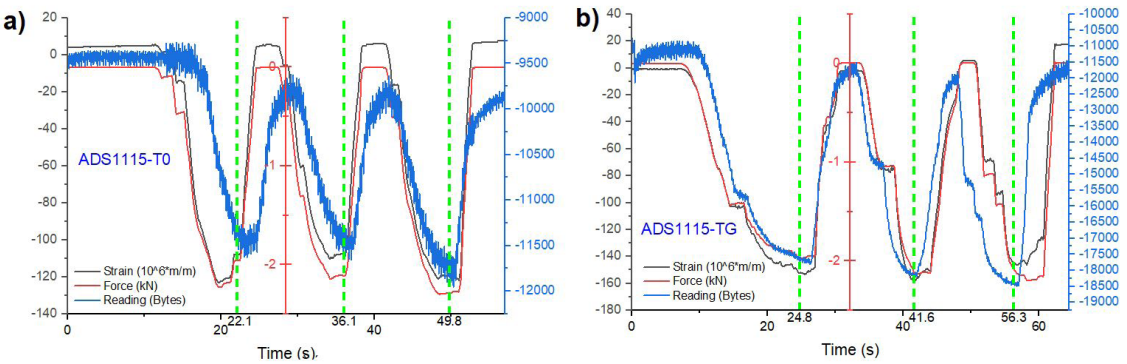

Figure 14. Arduino with ADS1115 module in compression test with mix proportions T0 (a) and TG (b).

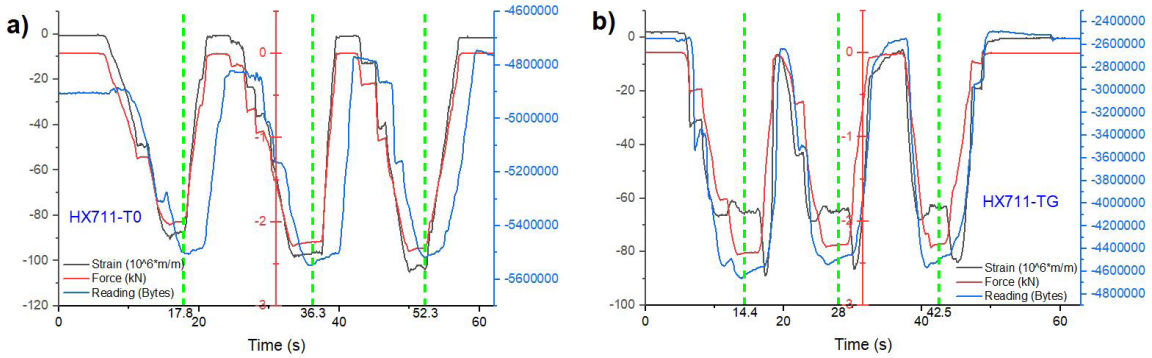

Figure 15. Arduino with HX711 module in compression test with mix proportions T0 (a) and TG (b).

Table 4. Sensitivity analysis with different devices (Arduino, ADS1115 and HX711).

Device	Sample	Figure	Time (s)	Peak Value		Sensitivity Equation 6 (Bytes/MPa)
				Δ Stress (MPa)	Δ Bytes	
Arduino	T0	13a	12.3	1.39	24	17.3
			28.3	1.31	26	19.9
			42.7	1.64	34	20.8
	TG	13b	24.3	1.22	31	25.4
			38.7	1.06	37	35.0
			60.6	1.26	29	23.1
ADS1115	T0	14a	22.1	1.22	1,941	1,585.4
			36.1	1.32	1,926	1,459.8
			49.8	1.43	2,430	1,699.2
	TG	14b	24.8	1.23	6,810	5,534.5
			41.6	1.32	7,390	5,583.3
			56.3	1.31	7,574	5,803.0
HX711	T0	15a	17.8	1.24	592,736	476,522.1
			36.3	1.40	635,674	454,477.5
			52.3	1.42	609,341	428,604.6
	TG	15b	14.4	1.49	2,086,021	1,404,446.1
			28.0	1.42	1,940,115	1,362,089.5
			42.5	1.42	1,946,317	1,370,129.0

Table 5. ANOVA between different devices (Arduino, ADS1115 and HX711).

Comparison		Degree of freedom	Sum of Squares	Mean Square	F*	p-value
Arduino *vs.* ADS1115	Model	3	2.11059E7	6.33176E7	2423.578	3.5896E-12
	Error	8	8708.56192	69668.49538		
Arduino *vs.* HX711	Model	3	3.80263E12	1.26754E12	4688.935	2.5680E-13
	Error	8	2.16261E9	2.70326E8		
HX711 *vs.* ADS1115	Model	3	3.78298E12	1.26099E12	4664.552	2.6221E-13
	Error	8	2.16268E9	2.70335E8		

*F is the ratio between Mean Squares

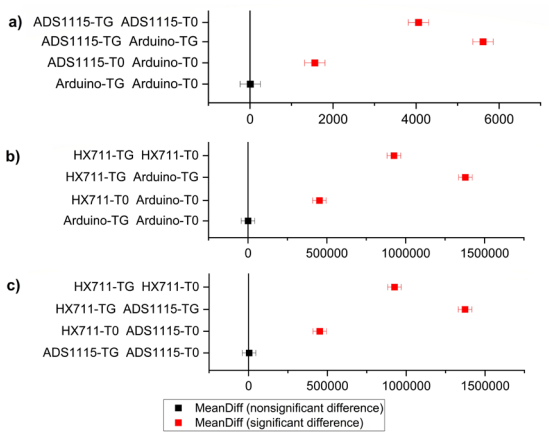

Figure 16. Tukey test between Arduino-ADS1115 (a), Arduino-HX711 (b), and ADS1115-HX711 (c).

with the reference DAQ. In these tests, the specimens (T0 and TG) remained without mechanical load during the period of data acquisition (approximately 600 seconds).

In the case of the mix proportion T0, it was graphically observed (Figure 19) that the stabilization of the voltage measurements had begun in both cases (prototype and reference DAQ) between 100 and 200 seconds. Figure 20 shows the percentage of variation stabilization of the voltage measurements, calculated in an interval of 10 seconds. Results show that in the case of the reference DAQ, stabilization (<2%, yellow line) occurred in about 78.6 seconds (Figure 20a). The same stabilization (<2%, yellow line), but in the prototype, occurred in about 147.2 seconds (Figure 20b).

For the specimen composed by mix proportion TG, it was also graphically observed (Figure 21) that the stabilization of the voltage measurements had begun in both cases (prototype and reference DAQ) between 100 and 200 seconds. Results show that in the case of the reference DAQ, stabilization (<2%, yellow line) occurred in about 110.9 seconds (Figure 22a). The same stabilization (<2%, yellow line), but in the prototype, occurred in about 212.6 seconds (Figure 22b).

Before the piezoresistive tests with the prototype, tests were done only with the reference DAQ to establish a reference parameter for the piezoresistivity effect in the specimens (T0 and TG). The results of these measurements are shown in Figure 23.

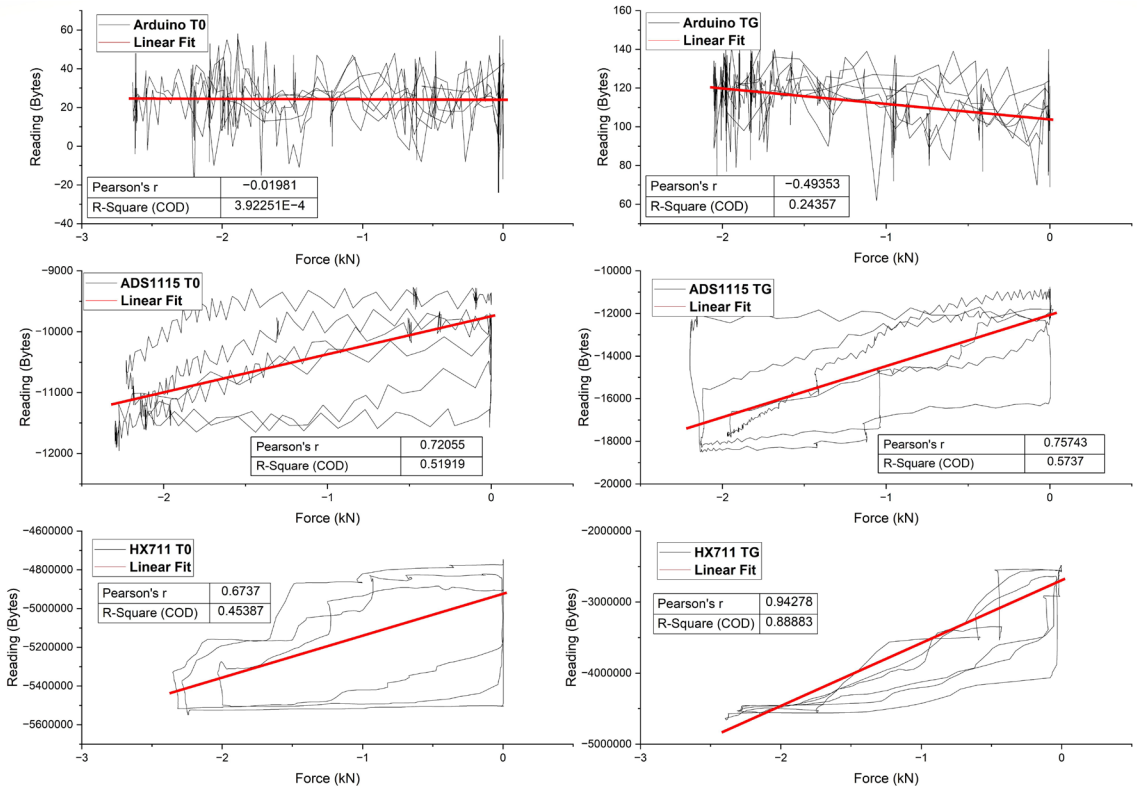

Figure 17. Correlations analysis (Pearson's r and R-Square) with different devices (Arduino, ADS1115 and HX711).

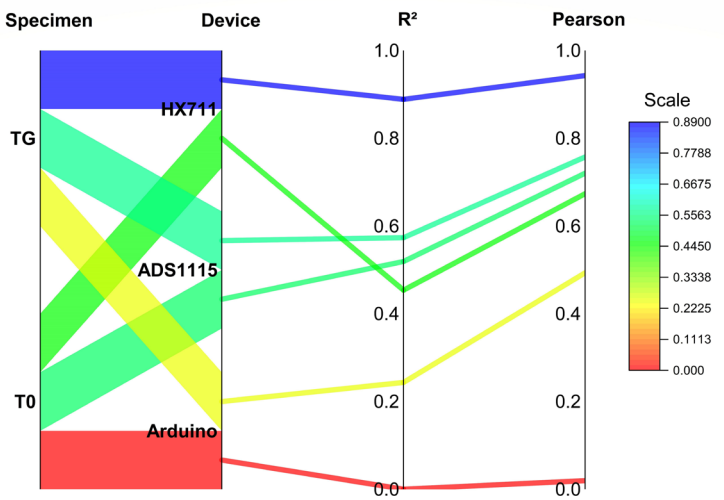

Figure 18. Graphical comparison between correlation analyses with different devices (Arduino, ADS1115 and HX711).

Then, the tests were performed where the acquisition of the FCR was done with the developed prototype and the mechanical parameters (force and strain) with the reference DAQ. The results of these measurements are shown in Figure 24.

Graphically, it was possible to observe that the majority of the results in Figures 23 and 24 showed a good piezoresistive effect (FCR) response to the mechanical parameters (force and strain). Some unsatisfactory FCR results (Figure 24b) suggest that these are not problems directly related to the developed

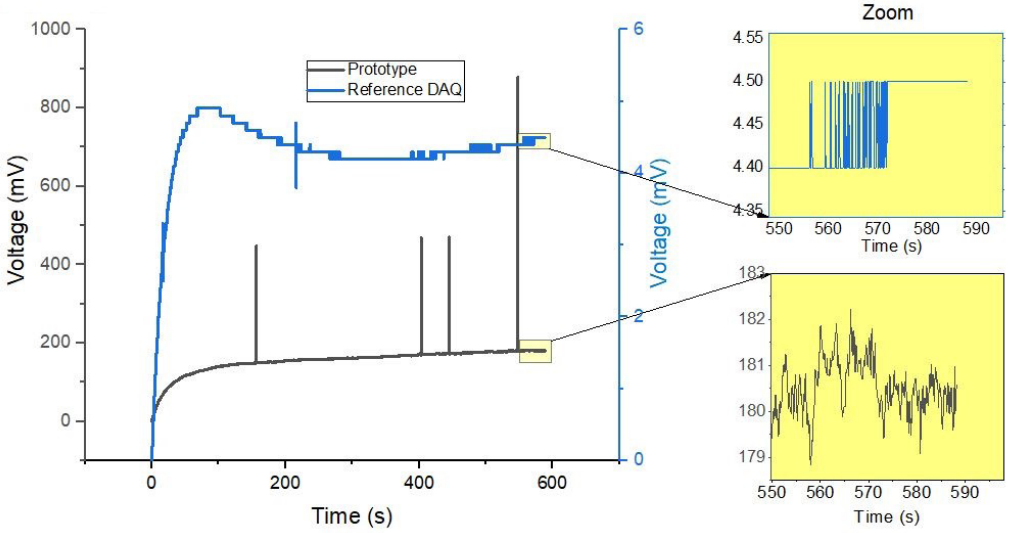

Figure 19. Polarization effect between prototype and reference DAQ with mortar T0.

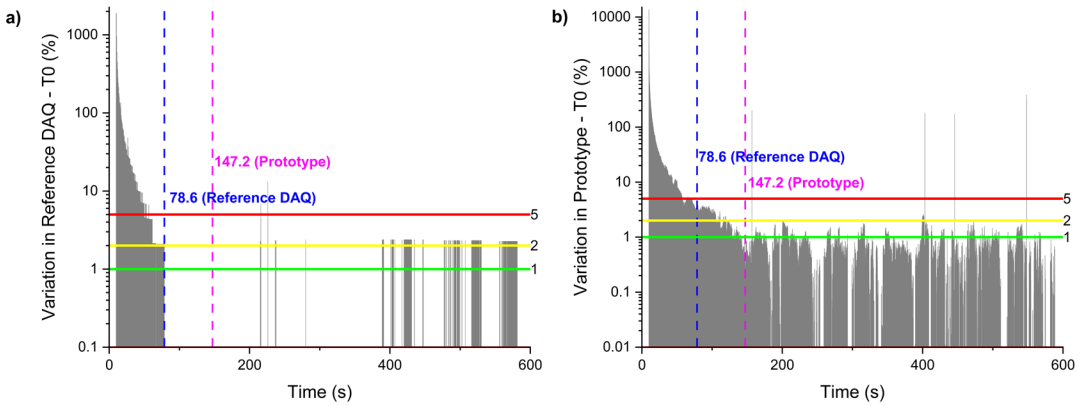

Figure 20. Variation of the polarization effect in an interval of 10 seconds with mortar T0.

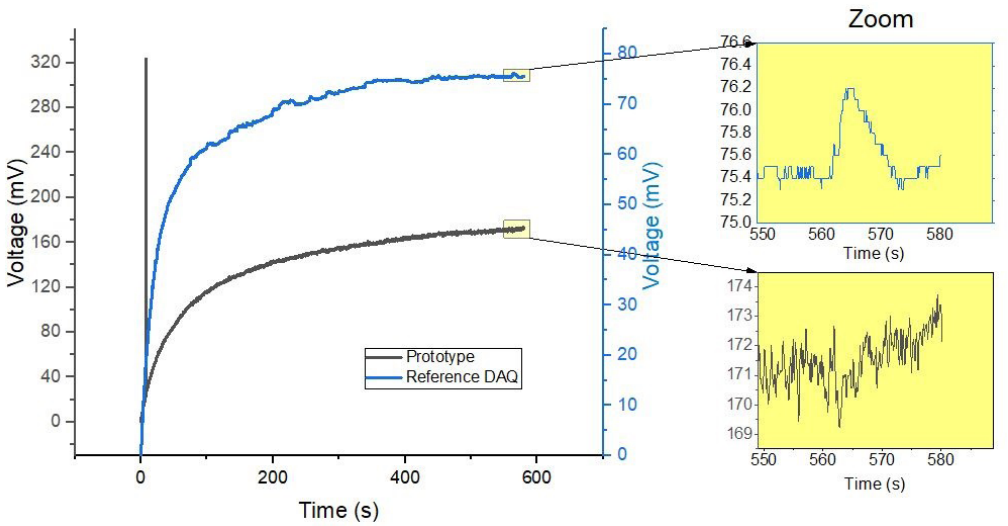

Figure 21. Polarization effect between prototype and reference DAQ with mortar TG.

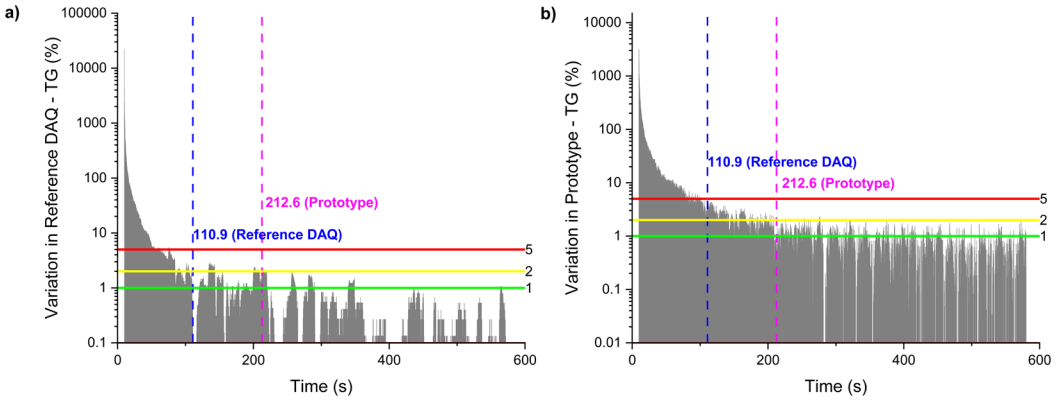

Figure 22. Variation of the polarization effect in an interval of 10 seconds with mortar TG.

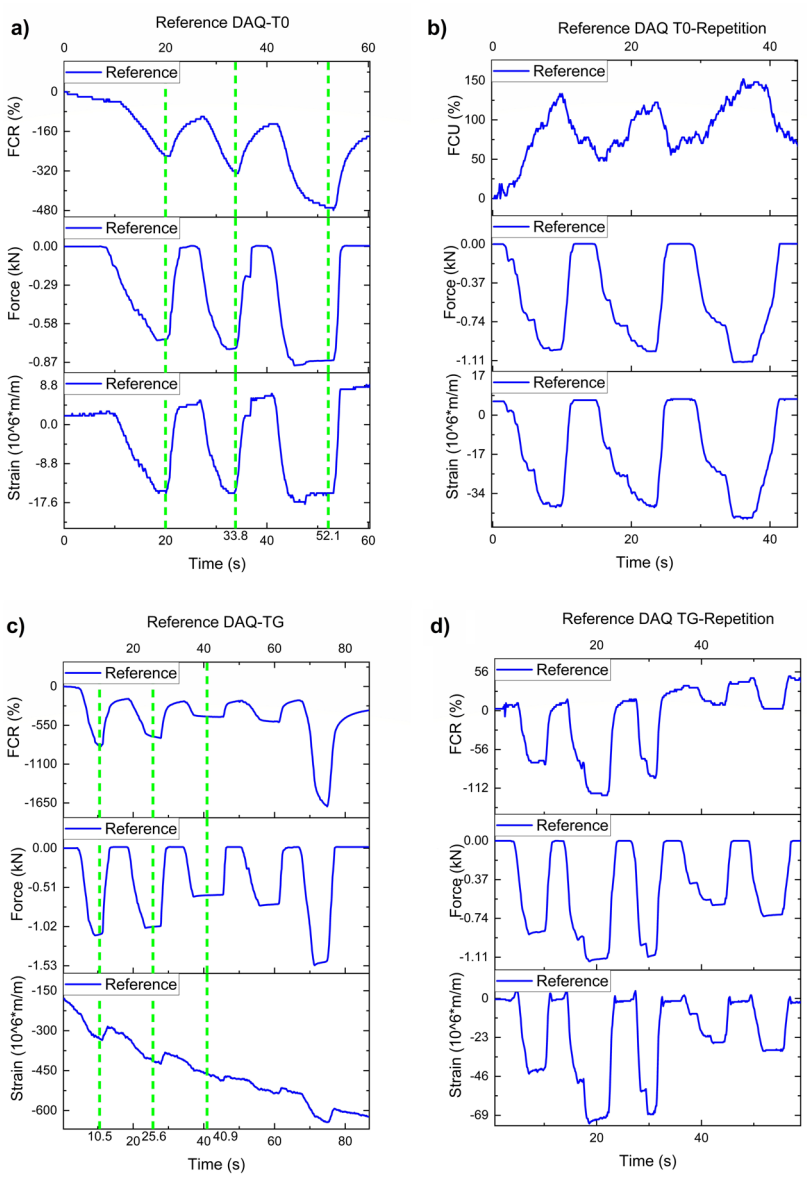

Figure 23. Comparative results between FCR and mechanical parameters, using the reference DAQ.

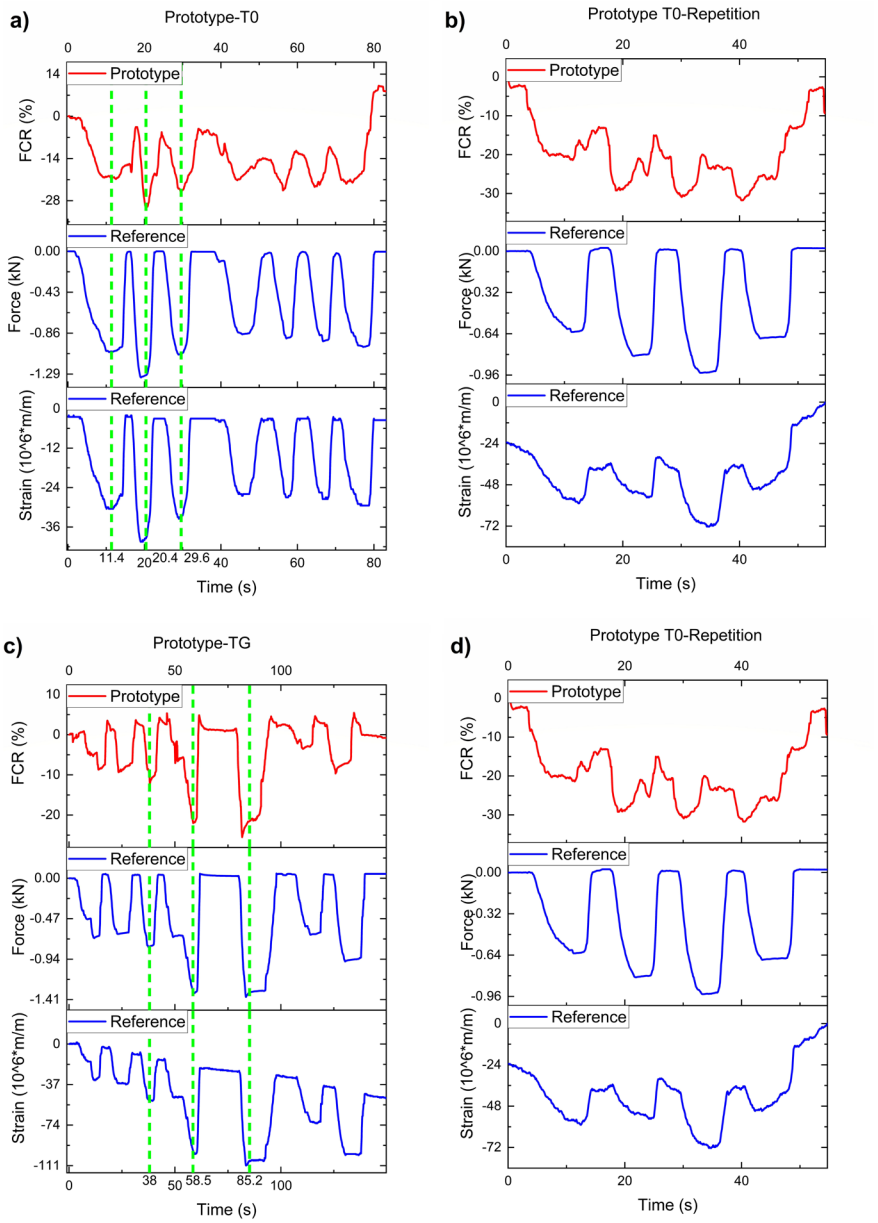

Figure 24. Comparative results between FCR and mechanical parameters, using the developed prototype and the reference DAQ.

prototype, as they were also observed (strain) in the case of using the reference DAQ. Another expected result was that in the case of the mix T0, thus, without the addition of graphite, there would be less response to the piezoresistive effect than in the case of the mix TG with the addition of graphite, due to the improvement in the conductivity of the composite.

The results of the sensitivity analysis of the reference DAQ and prototype (green lines in Figures 23 and 24), show in Table 6 that there is no good sensitivity in the use of the prototype, as found in the preliminary tests. These results only showed a difference in sensitivity between the mix proportions T0 and TG.

The analysis of variance (one-way) was performed between the reference DAQ and prototype, using the sensitivity values from Table 6. The results are shown in Table 7, indicating that some means are different (p-value<0.05) at a level of 95% significance.

The results of Tukey's Test of the sensitivity values between the reference DAQ and prototype showed (Figure 25) a significant difference in mean. However, this result was not desirable, because it indicated an unsatisfactory performance when compared with the preliminary results. In the case of the reference DAQ, these results showed a difference in sensitivity between the mix proportions T0 and TG.

The results of Pearson's and R-squared in Figures 26 and 27 show, in general, that the mix proportion with graphite (TG) had a better correlation than without graphite (T0), when the prototype or the reference DAQ are used.

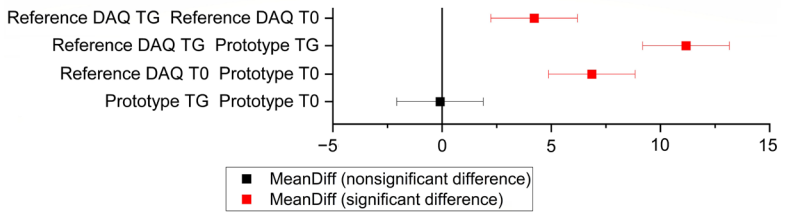

Figure 25. Tukey Test between prototype and reference DAQ.

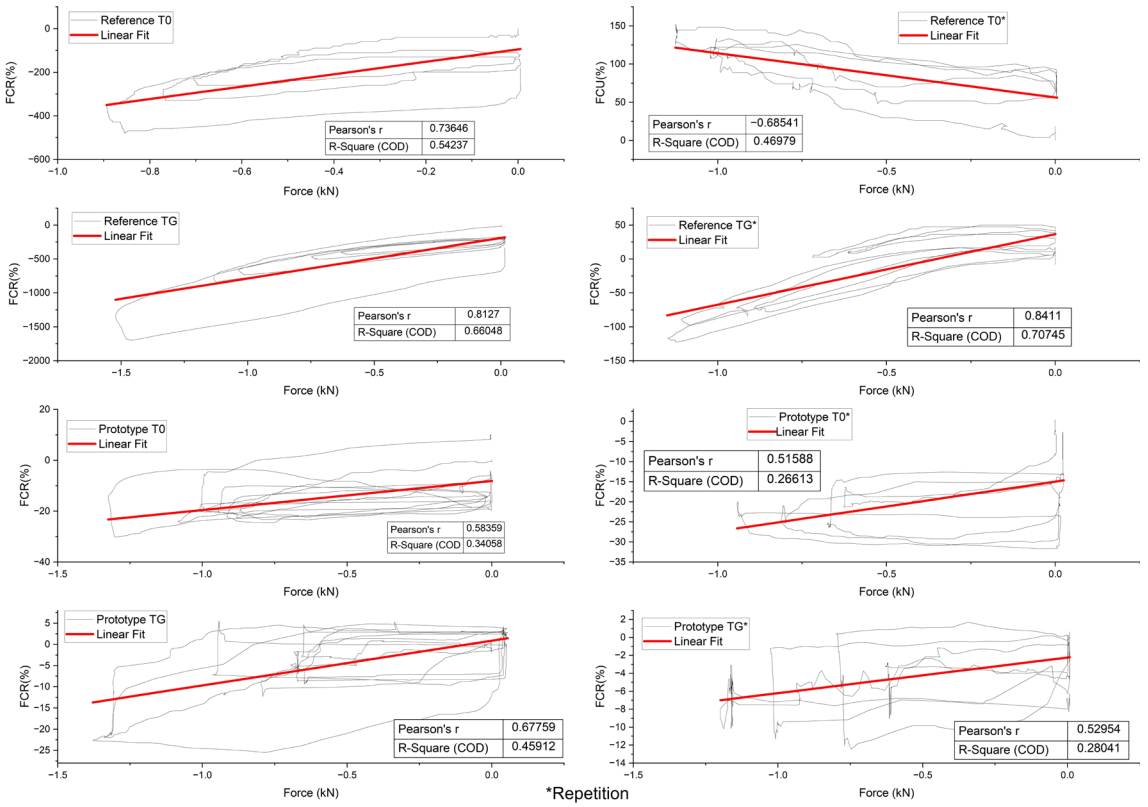

Figure 26. Correlations analysis (Pearson's r and R-Square) between prototype and reference DAQ.

Table 6. Sensitivity analysis with prototype and reference DAQ.

Device	Sample	Figure	Peak Value			Sensitivity Equation 7 (MPa^{-1})
			Time (s)	Δ Stress (MPa)	FCR (%)	
Reference	T0	23a	20.0	0.44	259.68	5.97
			33.8	0.48	329.52	6.90
			52.1	0.54	469.09	8.76
	TG	23c	10.5	0.70	843.04	12.03
			25.6	0.64	708.38	11.10
			40.9	0.38	426.75	11.15
Prototype	T0	24a	11.4	0.66	20.39	0.31
			20.4	0.81	30.16	0.37
			29.6	0.67	24.64	0.37
	TG	24c	38.0	0.49	11.98	0.24
			58.5	0.83	22.00	0.27
			85.2	0.83	21.47	0.26

Table 7. ANOVA between prototype and reference DAQ.

Comparison		Degree of freedom	Sum of Squares	Mean Square	F*	p-value
Prototype *vs.* Ref. DAQ	Model	3	270.37094	90.12365	157.0501	1.89956E-7
	Error	8	4.59082	0.57385		

*F is the ratio between Mean Squares

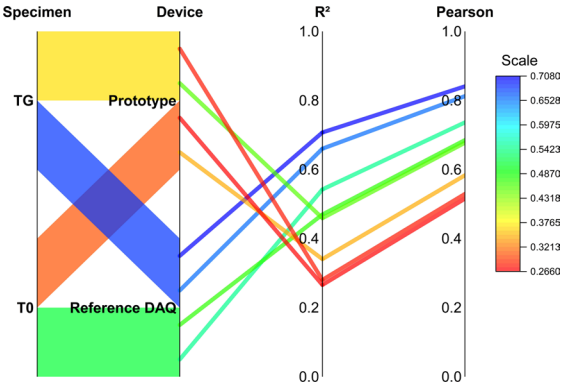

Figure 27. Graphical comparison between correlation analyses of the prototype and reference DAQ.

5. Conclusions

Based on the results obtained, especially the sensitivity analysis and the good correlation between the measurements made by the Arduino with the ADC's modules in comparison to the reference DAQ, it was concluded that low-cost technologies applied to the monitoring of SSCCs have significant potential to be used. Although at the moment limited to the field of scientific research. However, further studies and consequent advances can provide the effective use of devices like this in real construction.

Still from the results, we can specifically highlight that:

- Arduino with 10 bits needs an ADC module of 16 bits or greater to be used in SSCCs piezoresistive analysis;
- Although the sample without graphite (T0) showed some piezoresistive response, it was not better than the sample with graphite (TG), which showed better sensitivity and a better correlation between FCR and strain;
- The decrease in quality of the results between the use of the Arduino with the HX711 module and the developed prototype may be associated with several factors. For example, use of the reference resistors and the capacitor;
- Reducing the limitations in the use of Arduino in prototypes similar to this one demand more tests. This can include tests with different conductive materials in addition to graphite, as well as different loading conditions such as tension and bending moment.

In addition to the low-cost of developing the prototype, it was also found that the prototype is relatively easy to use, given its friendly interface, promoted by the operation through an app on a smartphone. This integration of materials and structures with Arduino and a smartphone is also a good fit for goals like the Internet of Things (IoT) and smart cities.

Finally, making the codes and schemes for the development of the prototype in question open-source allows other researchers to reproduce it for use in their research, in addition to collaborating on its improvement.

6. Acknowledgments

CAPES (Coordenação de Aperfeiçoamento de Pessoal de Nível Superior), Brasil - Financing Code 001; CNPq (Conselho Nacional de Desenvolvimento Científico e Tecnológico) - Prof. Luísa Andréia Gachet (310375/2020-7) e Prof. Rosa Cristina Cecche Lintz (310376/2020-3).

7. References

1. Hong W, Lv K, Jiang Y, Yang C, Wu Z, Hu X, et al. Self-sensing and quantitative assessment of prestressed concrete structures based on distributed long-gauge fiber Bragg grating sensors. J Intell Mater Syst Struct. 2018;29(9):1974-85.
2. Dong W, Li W, Tao Z, Wang K. Piezoresistive properties of cement-based sensors: review and perspective. Constr Build Mater. 2019;203:146-63.
3. Kekez S, Kubica J. Connecting concrete technology and machine learning: proposal for application of ANNs and CNT/concrete composites in structural health monitoring. RSC Advances. 2020;10(39):23038-48.
4. Maier M. The effect of moisture and reinforcement on the Self-sensing properties of hybrid-fiber-reinforced concrete. Eng Res Express. 2020;2(2):025026.
5. Sarwary MH, Yıldırım G, Al-Dahawi A, Anıl Ö, Khiavi KA, Toklu K, et al. Self-sensing of flexural damage in large-scale steel-reinforced mortar beams. ACI Mater J. 2019;116(4):209-21.
6. Chung DDL. Self-sensing concrete: from resistance-based sensing to capacitance-based sensing. Int J Smart Nano Mater. 2020;12(1):1-19.
7. Segura I, Faneca G, Torrents JM, Aguado A. Self-sensing concrete made from recycled carbon fibres. Smart Mater Struct. 2019;28(10):105045.
8. Chen PW, Chung DDL. Carbon fiber reinforced concrete for smart structures capable of non-destructive flaw detection. Smart Mater Struct. 1993;2(1):22-30.
9. Sofi A, Jane Regita J, Rane B, Lau HH. Structural health monitoring using wireless smart sensor network – An overview. Mech Syst Signal Process. 2022;163:108113.
10. Rovnaník P, Kusák I, Bayer P, Schmid P, Fiala L. Electrical and self-sensing properties of Alkali-activated slag composite with graphite Filler. Materials. 2019;12(10):1616.
11. Ozdagli AI, Liu B, Moreu F. Low-cost, efficient wireless intelligent sensors (LEWIS) measuring real-time reference-free dynamic displacements. Mech Syst Signal Process. 2018;107:343-56.
12. Shankar NVS, Chand AG, Rao KH, Sai KP. Low cost vibration measurement and optimization during turning process. Adv Mat Res. 2018;1148:103-8.
13. Gupta V, Sharma M, Pachauri RK, Babu KND. A low-cost real-time IoT enabled data acquisition system for monitoring of PV system. Energy Sources A Recovery Util Environ Effects. 2020;43(20):2529-43.

14. Nunes DS, Brito JLV, Doz GN. A low-cost data acquisition system for dynamic structural identification. IEEE Instrum Meas Mag. 2019;22(5):64-72.
15. Silva JBLP, Jacintho AEPGA, Forti NCS, Pimentel LL, Branquinho OC. Desenvolvimento de sistema de baixo custo para monitoramento de integridade estrutural. Materia. 2019;24(4):e12528.
16. Malik H, Khattak KS, Wiqar T, Khan ZH, Altamimi AB. Low cost internet of things platform for structural health monitoring. In: 2019 22nd International Multitopic Conference (INMIC); 2019; Islamabad, Pakistan. Proceedings. New York: IEEE; 2019. p. 1-7.
17. Patel T, Jain A, Gameti D, Patel U, Parekh R. Remote structural health monitoring system for bridges. In: IEEE International Students' Conference on Electrical, Electronics and Computer Science (SCEECS); 2020; Bhopal, India. Proceedings. New York: IEEE; 2020. p. 1-4.
18. Khan SM, Hanif MU, Khan A, Hassan MU, Javanmardi A, Ahmad A. Damage assessment of reinforced concrete beams using cost-effective MEMS accelerometers. Structures. 2022;41:602-18.
19. Serdjuks D, Kurtenoks V, Tatarinovs A, Buka-Vaivade K, Lapkovskis V, Mironovs V, et al. Non-model vibration analysis method for health monitoring of structural joints. Procedia Struct Integr. 2022;37:555-62.
20. Misra D, Das G, Das D. An IoT based building health monitoring system supported by cloud. J Reliab Intell Environ. 2020;6(3):141-52.
21. Buckley T, Ghosh B, Pakrashi V. Edge Structural Health Monitoring (E-SHM) using low-power wireless sensing. Sensors. 2021;21(20):6760.
22. Hu W, Ma X. Research on design and development of home virtual system based on internet of things system. Microprocess Microsyst. 2021;82:103857.
23. Ghatak B, Banerjee S, Ali SB, Das N, Tudu B, Pramanik P, et al. Development of a low-cost portable aroma sensing system for identifying artificially ripened mango. Sens Actuators A Phys. 2021;331:112964.
24. Podder AK, Bukhari AA, Islam S, Mia S, Mohammed MA, Kumar N, et al. M, Cengiz K, Abdulkareem KH. IoT based smart agrotech system for verification of Urban farming parameters. Microprocess Microsyst. 2021;82:104025.
25. Wang M, Koo KY, Liu C, Xu F. Development of a low-cost vision-based real-time displacement system using Raspberry Pi. Eng Struct. 2023;278:115493.
26. Harshitha C, Alapati M, Chikkakrishna NK. Damage detection of structural members using internet of things (IoT) paradigm. Mater Today Proc. 2021;43:2337-41.
27. Chang HF, Shokrolah SM. Integration with 3D visualization and IoT-based sensors for real-time structural health monitoring. Sensors. 2021;21(21):6988.
28. Andrzejczak A, Łęczycki P, Wojtera M, Pietrzak P, Pękosławski B, Napieralski A. Architecture of wireless vehicle weight measurement system for structural health monitoring in civil engineering application. Int J Distrib Sens Netw. 2015;11(8):02545.
29. Cardona-Vivas N, Correa MA, Colorado HA. Multifunctional composites obtained from the combination of a conductive polymer with different contents of primary battery waste powders. Sustainable Mater Technol. 2021;28:e00281.
30. Birgin HB, D'alessandro A, Favaro M, Sangiorgi C, Laflamme S, Ubertini F. Field investigation of novel self-sensing asphalt pavement for weigh-in-motion sensing. Smart Mater Struct. 2022;31(8):085004.
31. Kondaveeti HK, Kumaravelu NK, Vanambathina SD, Mathe SE, Vappangi S. A systematic literature review on prototyping with Arduino: applications, challenges, advantages, and limitations. Comput Sci Rev. 2021;40:100364.
32. Nalon GH, Ribeiro JCL, Pedroti LG, Araújo END, Carvalho JMF, Lima GES, et al. Residual piezoresistive properties of mortars containing carbon nanomaterials exposed to high temperatures. Cement Concr Compos. 2021;121:104104.
33. Lima GES, Nalon GH, Santos RF, Ribeiro JCL, Carvalho JMF, Pedroti LG, et al. Microstructural investigation of the effects of carbon black nanoparticles on hydration mechanisms, mechanical and piezoresistive properties of cement mortars. Mater Res Ibero-Am J Mater. 2021;24(4):1-12.
34. Abedi M, Fangueiro R, Correia AG. Effects of electrodes layout and filler scale on percolation threshold and piezoresistivity performances of a cementitious-based geocomposite. Nanomaterials. 2022;12(10):1734.
35. Ceylan H, Yavas S, Dong L, Jiao Y, Yang S, Kim S, et al. Development of a wireless MEMS multifunction sensor system and field demonstration of embedded sensors for monitoring concrete pavements, volume I. Iowa: Institute for Transportation, Iowa State University; 2016. 219 p. (Trans Project Reports).
36. Wang L, Aslani F. Mechanical properties, electrical resistivity and piezoresistivity of carbon fibre-based self-sensing cementitious composites. Ceram Int. 2021;47(6):7864-79.
37. Chung DDL. A critical review of piezoresistivity and its application in electrical-resistance-based strain sensing. J Mater Sci. 2020;55(32):15367-96.
38. Lee SY, Le HV, Kim DJ. Self-stress sensing smart concrete containing fine steel slag aggregates and steel fibers under high compressive stress. Constr Build Mater. 2019;220:149-60.
39. Yoo DY, You I, Lee SJ. Electrical properties of cement-based composites with carbon nanotubes, graphene, and graphite nanofibers. Sensors. 2017;17(5):1064.
40. Wang L, Aslani F. A review on material design, performance, and practical application of electrically conductive cementitious composites. Constr Build Mater. 2019;229:116892.
41. Monteiro AO, Loredo A, Costa PMFJ, Oeser M, Cachim PM. A pressure-sensitive carbon black cement composite for traffic monitoring. Constr Build Mater. 2017;154:1079-86.
42. Dehghani A, Aslani F. Piezoelectric behaviour of hybrid engineered cementitious composites containing shape-memory alloy, steel, and carbon fibres under compressive stress cycles. Constr Build Mater. 2021;273:121671.
43. Demircilioğlu E, Teomete E, Ozbulut OE. Characterization of smart brass fiber reinforced concrete under various loading conditions. Constr Build Mater. 2020;265:120411.
44. Madbouly AI, Mokhtar MM, Morsy MS. Evaluating the performance of rGO/cement composites for SHM applications. Constr Build Mater. 2020;250:118841.
45. Konkanov M, Salem T, Jiao P, Niyazbekova R, Lajnef N. Environment-friendly, self-sensing concrete blended with byproduct wastes. Sensors. 2020;20(7):1925.
46. D'Alessandro A, Ubertini F, Materazzi AL, Porfiri M. Electrical modelling of carbon nanotube cement-based sensors for structural dynamic monitoring. AIP Conf Proc. 2014;1603(1):23-30.
47. Dehghani A, Aslani F. Piezoresistive sensing of cementitious composites reinforced with shape memory alloy, steel, and carbon fibres. Constr Build Mater. 2021;267:121046.
48. Nalon GH, Ribeiro JCL, Araújo END, Pedroti LG, Carvalho JMF, Santos RF, et al. Effects of different kinds of carbon black nanoparticles on the piezoresistive and mechanical properties of cement-based composites. J Build Eng. 2020;32:101724.
49. Downey A, D'Alessandro A, Ubertini F, Laflamme S, Geiger R. Biphasic DC measurement approach for enhanced measurement stability and multi-channel sampling of self-sensing multi-functional structural materials doped with carbon-based additives. Smart Mater Struct. 2017;26(6):065008.
50. Kouchakzadeh S, Narooei K. Simulation of piezoresistance and deformation behavior of a flexible 3D printed sensor

considering the nonlinear mechanical behavior of materials. Sens Actuators A Phys. 2021;332:113214.
51. Lee SH, Kim S, Yoo DY. Hybrid effects of steel fiber and carbon nanotube on Self-sensing capability of ultra-high-performance concrete. Constr Build Mater. 2018;185:530-44.
52. Sanli A, Benchirouf A, Müller C, Kanoun O. Piezoresistive performance characterization of strain sensitive multi-walled carbon nanotube-epoxy nanocomposites. Sens Actuators A Phys. 2017;254:61-8.
53. Kim TU, Le HV, Park JW, Eock SK, Jang Y, Kim DJ. Development of a smart concrete block with an eccentric load sensing capacity. Constr Build Mater. 2021;306:124881.
54. Dong W, Li W, Wang K, Luo Z, Sheng D. Self-sensing capabilities of cement-based sensor with layer-distributed conductive rubber fibres. Sens Actuators A Phys. 2020;301:111763.
55. Frąc M, Szudek W, Szołdra P, Pichór W. The applicability of shungite as an electrically conductive additive in cement composites. J Build Eng. 2022;45:103469.
56. ABNT: Associação Brasileira de Normas Técnicas. ABNT NBR 16605: Portland cement and other powdered material: determination of the specific gravity. Rio de Janeiro: ABNT; 2017.
57. ABNT: Associação Brasileira de Normas Técnicas. ABNT NBR 16916: aggregates: determination of the unit weight and air-void contents. Rio de Janeiro: ABNT; 2021.
58. ABNT: Associação Brasileira de Normas Técnicas. ABNT NBR 17054: aggregates: determination of granulometric composition: test method. Rio de Janeiro: ABNT; 2022.
59. ABNT: Associação Brasileira de Normas Técnicas. ABNT NBR 16868-2: structural masonry part 2: execution and site control. Rio de Janeiro: ABNT; 2020.
60. D'Alessandro A, Tiecco M, Meoni A, Ubertini F. Improved strain sensing properties of cement-based sensors through enhanced carbon nanotube dispersion. Cement Concr Compos. 2021;115:103842.
61. Silva JBLP, Lintz RCC, Gachet LA. The utilization of pearson's method to analyze piezoresistive effect in self-sensing cement composite with graphite. Mater Res. 2022;25:e20220051.
62. Suchorzewski J, Prieto M, Mueller U. An experimental study of self-sensing concrete enhanced with multi-wall carbon nanotubes in wedge splitting test and DIC. Constr Build Mater. 2020;262:120871.
63. Zhang L, Ding S, Han B, Yu X, Ni YQ. Effect of water content on the piezoresistive property of smart cement-based materials with carbon nanotube/nanocarbon black composite filler. Compos, Part A Appl Sci Manuf. 2019;119:8-20.
64. Tao J, Wang J, Zeng Q. A comparative study on the influences of CNT and GNP on the piezoresistivity of cement composites. Mater Lett. 2020;259:126858.
65. Tao J, Wang X, Wang Z, Zeng Q. Graphene nanoplatelets as an effective additive to tune the microstructures and piezoresistive properties of cement-based composites. Constr Build Mater. 2019;209:665-78.
66. Nalon GH, Ribeiro JCL, Pedroti LG, Araújo END, Carvalho JMF, Lima GES, et al. Self-sensing mortars: effect of moisture and nanocarbon black content. ACI Mater J. 2021;118(3):131-41.

Supplementary material

The following online material is available for this article:

Programming codes